Eur Biophys J (2010) 39:1155–1165
DOI 10.1007/s00249-009-0568-0

ORIGINAL PAPER

X-ray scattering studies of model lipid membrane interacting with purothionin provide support for a previously proposed mechanism of membrane lysis

Jaroslaw Majewski · Boguslaw Stec

Received: 21 June 2009 / Revised: 15 November 2009 / Accepted: 19 November 2009 / Published online: 10 December 2009

Abstract Thionins, ubiquitous plant toxins, are believed to act by lysing the membrane of pathogenic organisms. Several competing mechanisms were proposed for the lysis of phospholipid membranes by the toxins. In order to study in more detail the proposed mechanisms and possibly resolve among the competing proposals, the interactions of purothionins with a model lipid membrane in the form of a monolayer were studied. The monolayer formed at the air-water interface was studied by synchrotron X-ray reflectivity and grazing incidents diffraction methods. The model membrane was composed of 90:10 mol% DPPC:DPPS (dipylmitoyl phosphatidylcholine:dipylmitoyl phosphatidylserine). The protein interaction with the monolayer disturbs the in-plane and out-of-plane order of phospholipids, increases the amount of the liquid phase of the monolayer, and increases the average surface area per alkyl chain. The results indicate that the protein is bound only transiently, and after ~4 h most of the properties of the monolayer are reminiscent of the pure DPPC monolayer suggesting partial withdrawal of DPPS. Obtained electron density distributions perpendicular to the membrane interface do not show any significant contribution from the adsorbed proteins, further supporting the withdrawal hypothesis.

J. Majewski
Manuel Lujan Jr. Neutron Scattering Center,
Los Alamos National Laboratory, MS-H805,
Los Alamos, NM 87545, USA

B. Stec (✉)
Infectious and Inflammatory Disease Center,
Burnham Institute for Medical Research,
10901 N. Torrey Pines Rd., La Jolla, CA 92037, USA
e-mail: bstec@burnham.org

Keywords Plant toxins · Thionins · Mechanism of toxicity · Membrane lysis · Grazing incidence diffraction (GIXD) · X-ray reflectivity · Langmuir monolayers · Air-water interface · Model biomembranes

Abbreviations

GIXD	Grazing incidence X-ray diffraction
XR	X-ray reflectivity
DPPC	Dipylmitoyl phosphatidylcholine
DPPS	Dipylmitoyl phosphatidylserine
PT	Purothionin

Introduction

Purothionins belong to the group of low molecular weight (~5 kDa) plant polypeptides, rich in disulfides, called thionins (Stec 2006; Bohlmann and Apel 1991; Carrasco et al. 1981). This family is composed of *Gramineae* toxins, the toxins of the extended cabbage family, and the homologous proteins from dicotyledonous plants (different species of mistletoe and *Pyrularia pubera*). Representative members of this family are α_1- and β-purothionins, α- and β-hordothionins, phoratoxin-A, *Pyrularia pubera* toxin, and viscotoxin-A3 (Fig. 1) (for a recent review, see Stec 2006). Despite small variations in length (45–47 amino acids), they share the same three-dimensional architecture and most likely the same mechanism of toxicity. Their wide distribution from endosperm to leaves and synthesis in response to bacterial invasion suggest an important role in defense against pathogenic invaders (Castro and Fontes 2005; Broekaert et al. 1997). Their toxic effect was

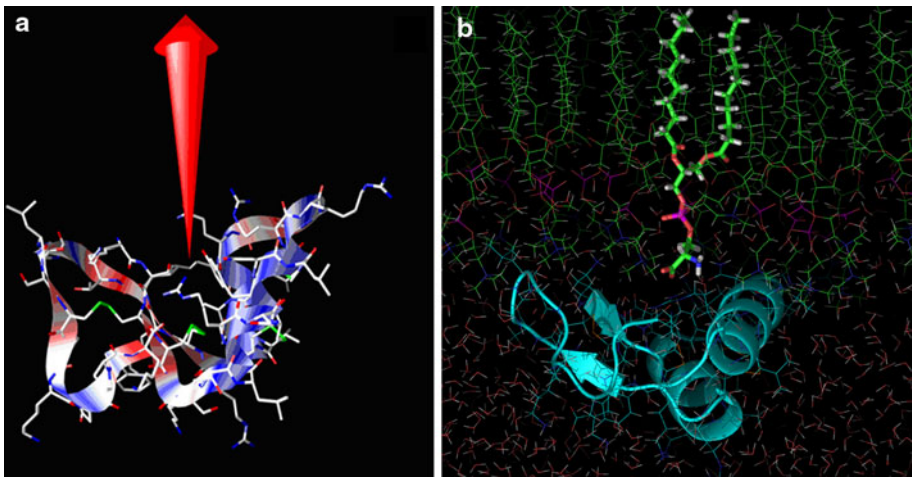

Fig. 1 **a** The ribbon representation of beta-purothionin superimposed onto a bond-stick model showing the distribution of positively charged amino acids. The *arrow* represents the vector of the electric field originating at the site of binding of a small molecule entity (glycerol, serine, phosphate, etc.) detected in each crystal structure of thionins (Rao et al. 1995; Stec et al. 1995; Debreczeni et al. 2003; Johnson et al. 2005) that is proposed to be the phospholipid binding suite. **b** Illustration of the possible attachment of the DPPS to the purothionin as represented by a snapshot of an MD simulation

postulated to arise from lysis of the membranes of the attacking cells (Castro and Fontes 2005; Garcia-Olmedo et al. 1998). Several mechanisms for cell membrane lysis were proposed including the formation of ion channels (Llanos et al. 2004; Hughes et al. 2000), rigidified lipid rafts (Thevissen et al. 1999; Giudici et al. 2003), and solubilization of membrane phospholipids (Stec et al. 2004), but the details remain unclear.

Permeabilization of the foreign cell membrane is the first step in the defense mechanism, and a variety of other secondary effects accompany cell lysis. Upon the introduction of toxins there is a depolarization of the membrane and Ca^{2+} ion permeability increases (Evans et al. 1989). Endogenous PLA2 (Angerhofer et al. 1990; Vernon and Bell 1992) and adenylate cyclase are activated (Huang et al. 1994). Protein kinase C is inhibited and DNA and RNA binding is detected (Li et al. 2002; Woynarowski and Konopa 1980) upon application of the toxins to different cell lines. All these events follow the disruption of the cell membrane, magnify the initial toxic effects, and lead to disruption of many crucial cell processes and ultimately to cell death. In this paper, we focus on the primary effect of the thionins, i.e., their function at the biological membrane. We investigated the changes in 2-D packing properties of a monolayer at the air-water interface consisting of a 90:10 mol% mixture of DPPC:DPPS upon introduction of $\sim$5 μM concentration of purothionin. We used such a monolayer as a mimic of the outer leaflet of the invading pathogen's cell membrane.

Materials

The lipid monolayers used in these studies were composed of 90:10 mol% of DPPC:DPPS [1,2-dipalmitoyl-*sn*-glycero-3-phosphocholine:1,2-dipalmitoyl-*sn*-glycero-3-(phospho-L-serine)]. DPPC and DPPS were obtained from Avanti Polar Lipids and were used without further purification. DPPC and DPPS lipids were dissolved in chloroform:methanol 90:10 vol% ($\sim$1.2 mg/ml). The stock solutions were used to obtain 90:10 mole ratio and deposited on an H_2O 50 mM Tris buffer subphase (pH = 8.2). Purothionin was purchased from SIGMA. Purothionin in powder form was solvated with buffer to a concentration of 1 mg/ml. The protein solution (5 ml) was then injected into the subphase (under the monolayer) to a final concentration of 20 mg/l ($\sim$5 μM). At this protein concentration the number of phospholipid molecules is smaller by several orders of magnitude than the number of protein molecules. The injection was performed in several points of the trough to yield a homogeneous protein concentration throughout the volume of the trough ($\sim$200 ml). Protein was allowed to incubate for $\sim$3 h before the first X-ray reflectivity (XR) and grazing incidence X-ray diffraction (GIXD) scans were measured. Throughout each experiment conducted at a temperature of 23°C the surface pressure of 20 mN/m was held constant. These conditions, although on the lower bound of the reported membrane surface pressures of 20–45 mN/m, approximate the surface pressure of a physiological cellular membrane as inferred from a number of experiments (Mansour and Zografi 2007). Additionally, at 20 mN/m the 90:10 mol%

DPPC:DPPS monolayer exhibits a significant amount of the gel-phase with in-plane ordering allowing grazing incidence diffraction to be measured.

All synchrotron X-ray measurements were carried out using the liquid surface diffractometer at the BW1 (undulator) beam line at HASYLAB, DESY (Hamburg, Germany). A temperature-controlled Langmuir trough equipped with a Wilhelmy balance for surface pressure measurements with a motorized barrier for surface pressure control was used. The trough was enclosed in a sealed, helium-filled canister where the low oxygen level was constantly monitored. The synchrotron X-ray beam was monochromated to a wavelength of $\lambda \sim 1.305$ Å by Laue reflection from a beryllium (200) monocrystal. The monochromatic beam was bent down to yield a glancing angle with the horizontal liquid surface by tilting the normal to the reflecting monocrystal planes away from the horizontal liquid surface plane.

X-ray reflectivity

The theory of X-ray reflectivity (XR) and grazing incidence X-ray diffraction (GIXD) has been presented in great detail elsewhere (Als-Nielsen et al. 1994) and only briefly is given here. Reflectivity, R, is defined as the intensity ratio of X-rays specularly scattered from a surface relative to the incident X-ray beam intensity. The reflectivity is measured as a function of wave-vector transfer $q_z = |\boldsymbol{k}_{\text{out}} - \boldsymbol{k}_{\text{in}}| = 4\pi\sin\theta/\lambda$, where θ is the angle of incidence and λ is the wavelength of the X-ray beam. The reflectivity curve contains information regarding the sample-normal profile of the in-plane average (over the footprint of the beam) of the electron densities. Reflectivities with q_z values from 0.01 to 0.8 Å^{-1} were measured using an NaI scintillation detector, and reasonable statistics were obtained to values of $R \sim 10^{-10}$. Typical scanning times for this q_z range were 30 min. The absolute reflectivity was derived by subtracting background followed by normalization to the incident beam flux. The data were reduced and plotted as R/R_F versus the perpendicular scattering vector, q_z (the division by Fresnel reflectivity, R_F, increases the visibility of the reflectivity profile by accounting for a sharp q_z^{-4} decrease in the reflectivity). The analysis of the measured reflectivity curves was performed using a free form cubic b-spline fitting routine (Hamley and Pedersen 1994) in which the coefficients in the series were determined by constrained nonlinear least-squares methods. The final solution with the lowest χ^2 was chosen. Confidence in these models was supported by the fact that the family of models deviating by a maximum of 5% of χ^2 showed no significant changes to the electron density profile.

Grazing incident X-ray diffraction

The dimension of the X-ray beam footprint on the liquid surface was $\sim 2 \times 50$ mm. For the GIXD experiments, the X-ray beam was adjusted to strike the surface at an incident angle θ of $\sim 0.11°$, which corresponds to a vertical momentum transfer vector $q_z = 0.85 q_c$, where $q_c = 0.0218$ Å^{-1} is the critical scattering vector for total external reflection from the liquid subphase (Fig. 2). At this angle the incident wave is totally reflected, while the refracted wave becomes evanescent traveling along the liquid surface thereby maximizing surface sensitivity. For in-plane diffraction measurements, a vertically placed Soller collimator giving a lateral resolution of $\Delta q_{xy} = 0.0075$ Å^{-1} was placed before a vertical one-dimensional position sensitive detector (PSD) with vertical acceptance $0 < q_z < 1.2$ Å^{-1}. This configuration allowed Bragg peak and Bragg rod measurements to be made simultaneously.

In three-dimensional (3D) crystals, diffraction maxima are observed for interplanar spacing d according to Bragg's law ($n\lambda = 2d\sin\theta$, n is an integer). In two-dimensional (2D) systems, the monolayers are a mosaic of 2D crystals with random orientation about the direction normal to the subphase and can therefore be described as 2D powders. Due to the lack of restriction on the scattering vector component q_z along the direction normal to the 2D crystal, Bragg scattering extends as continuous Bragg rods in reciprocal space (Als-Nielsen et al. 1994).

The scattered intensity was measured by scanning over a range of horizontal scattering vectors, $q_{xy} \sim 4\pi\sin\theta_{xy}/\lambda$, where $2\theta_{xy}$ is the angle between the incident and diffracted beam projected onto the horizontal plane, q_{xy} is

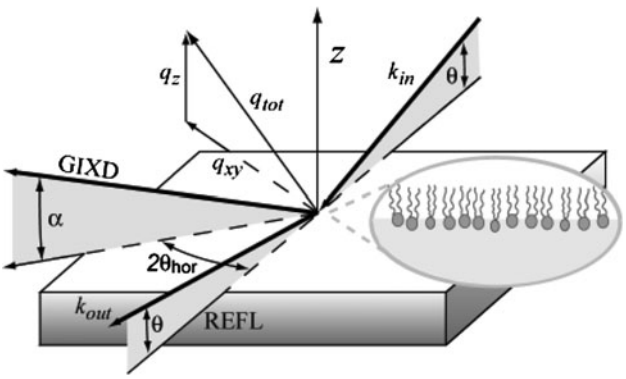

Fig. 2 The schematic representation of the experimental setup for the X-ray reflectivity (XR) and grazing incidence diffraction (GIXD) study on a phosphilipid monolayer. During the XR measurement, the $2\theta_{\text{hor}}$ angle is zero and the incident angle θ is varied. During GIXD, the angle of incidence, θ, of the X-ray beam is kept constant and less than the angle of total external reflection from the air-water interface

the combination of horizontal components q_x and q_y, and α_i and α_f are the incident and the reflected angles, respectively (Jensen et al. 2001). For details of the geometrical setup, see Fig. 2, and for an example of the resulting diffraction pattern, see Fig. 3. Bragg peaks were resolved in the q_{xy} direction and obtained by integrating the scattered intensity over channels along the z direction in the PSD. Conversely, the Bragg rod profiles were resolved in the q_z direction (i.e., along $q_z = 2\pi\sin(\theta)/\lambda$) and obtained by integrating the scattered intensity over q_{xy} corresponding to the Bragg peak. The q_{xy} positions of the maxima of the Bragg peaks allowed for the determination of the repeat distances d for the 2D lattice. The intensity distribution along the Bragg rod was analyzed to determine the direction and magnitude of the molecular tilt, the coherently scattering length of the molecule, L_c (Guinier 1963), and the magnitude of molecular motion or surface roughness, σ, of the crystallite (Debye–Waller factor) (Als-Nielsen et al. 1994).

Beam damage

X-rays with a wavelength of 1.305 Å (9.5 keV) can cause significant beam damage to the monolayer/protein sample. Overexposure can "burn" the sample, causing a change in the real space structure over time. To mitigate damage to the monolayer by X-rays, the oxygen content in the canister was kept below 1% and the sample was translated perpendicular to the beam (in between and during scans) and was only scanned once for all measurements reported.

Results

Area expansion analysis

At a constant surface pressure of 20 mN/m (Neville et al. 2008), purothionin's interaction with the monolayer resulted in an increase in the area of the monolayer film. The relative increase in the area per lipid molecule as toxin interacts at pH = 8.2 is shown in Fig. 4. The purothionin was injected at $t = 0$ min, yielding a monotonic increase in the area upon interaction. Between 170 and 230 (~3 h) min after injection, the first set of XR and GIXD experiments was performed. Slight vibrations caused by the moving parts of the spectrometer increased the ratio of area expansion. The area stopped expanding at around 230 min after injection. The second XR and GIXD scans were performed starting at 330 min (~6 h) after injection. The increase in area per molecule is due to changes in the physical characteristics of the monolayer. Contributing factors included a shift of phospholipids from the gel to liquid phase, packing inefficiencies of the lipids caused by the protein, or protein insertion into the lipid monolayer, or a combination of all.

GIXD and XR

The GIXD and XR data provide complementary information. GIXD provides information only about the ordered part of the monolayer. More specifically, the source of the diffraction is a lattice-like arrangement of the alkyl tails of

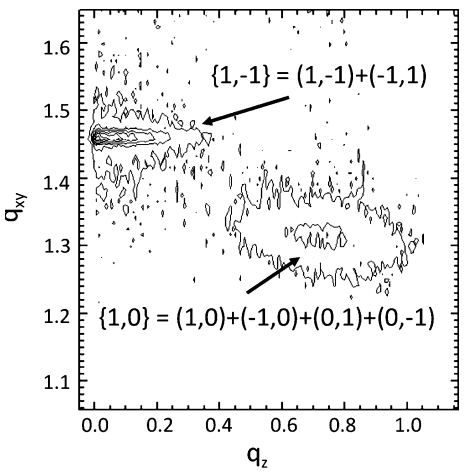

Fig. 3 An example of the GIXD results. A typical reciprocal space contour plot, $I(q_{xy}, q_z)$, obtained for the 90:10 mol% DPPC:DPPS phosphilipid monolayer incubated for ~6 h with purothionin injected into the water subphase. The diffraction originates from the order of the alkyl tails. Water surface (horizon) is at $q_z = 0$ Å^{-1}. Scattering vector q_{xy} is along the horizon and q_z is perpendicular to the monolayer. Two diffraction peaks are observed due to the distortion of the hexagonal unit cell of tilted alkyl tails. The Miller indices of the two reflections are indicated on the plot

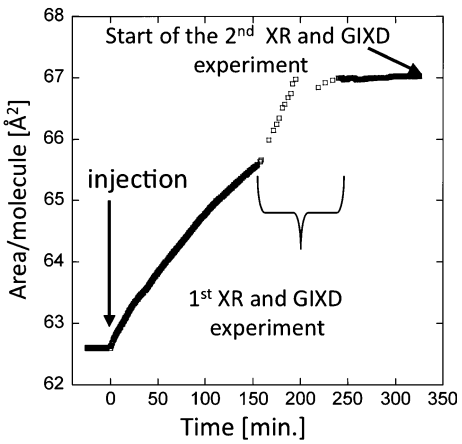

Fig. 4 The increase in the average area per DPPC:DPPS phospholipid molecule as a function of time. Time zero corresponds to the time of addition of the beta-purothionin to the subphase. Between ~170–230 min after injection, the first set of XR and GIXD experiments was performed. Slight vibrations caused by the moving spectrometer increased the ratio of area expansion. The area stopped expanding at around 230 min after injection. The second XR and GIXD scans were performed starting at 330 min after injection

the phospholipids. Diffraction from the lipid head-groups and 2-D arrangement of purothionins (both at small q_{xy} ranges) under the lipid monolayer was not observed.

In order to provide the controls and necessary base for investigating the changes caused by purothionin, we first investigated the pure DPPC, DPPS, and mixed 90:10 mol% DPPC:DPPS monolayers. All experiments were performed at 23°C and a constant surface pressure of 20 mN/m.

After characterization of the pure 90:10 mol% DPPC:DPPS monolayer, the protein was added to the water subphase. Addition of purothionin caused an increase in the area per molecule, and the global change took almost 4 h to be completed as indicated by the changes in area per lipid molecule (Fig. 4).

The analysis and comparison between GIXD spectra of pure DPPC, DPPS monolayers, and the 90:10 DPPC:DPPS mixed system at $\pi = 20$ mN/m and 23°C. (see Fig. 5 and Table 1 for details) showed numerous features. Alkyl tails of pure DPPC pack in a distorted hexagonal cell ($|\boldsymbol{a}| = |\boldsymbol{b}|$, $\gamma < 120°$) as indicated by the two in-plane diffraction peaks. The pure DPPC forms in-plane ordered islands characterized by the large L_{1-1} correlation length of 1,100 Å (comparable to the maximum coherence lengths one can resolve based on the lateral resolution of Δq_{xy}) but relatively small $L_{10,\ 01}$ correlation length (~78 Å).

Alkyl tails of the DPPS pack in a 2-D oblique unit cell ($|\boldsymbol{a}| \neq |\boldsymbol{b}|$, $\gamma < 120°$) as indicated by the three in-plane diffraction peaks (Fig. 5) and with smaller area per molecule than pure DPPC as indicated by higher q_{xy} positions of the diffraction peaks. The $L_{1,-1}$ coherence length gets smaller (~490 Å) while the coherence lengths along (1,0) and (0,1) crystallographic directions become longer (~120 and 140 Å) than for the pure DPPC monolayer.

As can be seen from the GIXD results, addition of 10 mol% of DPPS to DPPC creates the ordered 2-D structure with the following packing properties:

1. Alkyl tails pack in a distorted hexagonal cell as in the case of pure DPPC monolayer.
2. Resulting area per phospholipid molecule is between that of pure DPPC and pure DPPS, but it is not a linear combination of the areas per molecule of the pure components with the coefficients of mol% (Table 1). The 10 mol% of DPPS has much greater effect on the decreasing of the area per molecule (double size of the unit cell) as one would predict from the linear combination of unit cells dimensions of pure components.
3. The correlation length along the (1, −1) crystallographic direction becomes even longer than in the case of pure DPPC monolayer (~1,300 Å) although the $\text{FWHM}_{\text{meas}}$ of this diffraction peak is close to the instrumental resolution. The coherence lengths along the (1, 0) and (0, 1) directions resemble these of pure DPPC monolayer (75 Å).
4. Overall intensity of the diffraction peaks decreases substantially as compared to pure DPPC, testifying to less ordered material in the footprint of the beam.

GIXD spectra measured at ~3 and ~6 h after injection of 5 mg/250 ml purothionin to the mixed DPPC:DPPS, 90:10 mol%, show only small changes in the 2-D packing properties of the ordered portion of the monolayer (Fig. 6,

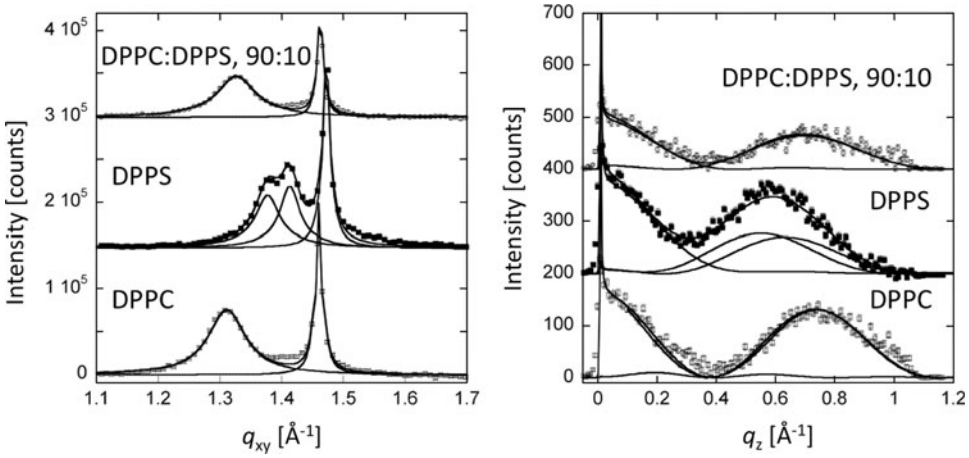

Fig. 5 GIXD profiles of pure DPPC, DPPS, and the 90:10 mol% DPPC:DPPS. *Left panel* represents Bragg peaks and the *right panel* shows the Bragg rods. *Solid lines* represent the fits to the measured profiles, and the molecular packing parameters used in the fitting are listed in Table 1. Bragg peaks were obtained by integrating over the (-0.05 Å$^{-1} \leq q_z \leq 1.2$ Å^{-1}) region, and each peak was fit using a Voigt function (*solid lines*). By integrating over the (1.15 Å$^{-1} \leq q_{xy} \leq 1.55$ Å^{-1}) region, the Bragg rods were fitted (*solid line*) by approximating the coherently scattering part of the alkyl tail by a cylinder of constant electron density. The sharp peak at $q_z = 0.01$ Å^{-1} is the so-called Yoneda-Vineyard peak, which arises from the interference between X-rays diffracted up into the monolayer and X-rays diffracted down and then reflected up by the interface. For clarity, both the Bragg peaks have been offset vertically by 1.5×10^5 counts and the Bragg rods by 200 counts

Table 1 GIXD parameters for the pure phospholipid and phospholipid plus protein

Composition	In-plane Bragg peaks (20 mN/m, H_2O, 50 mM TRIS buffer, pH 8.2, 23°C)										Out-of-plane Bragg rods (20 mN/m, H_2O, 50 mM TRIS buffer, pH 8.2, 23°C)			
	Observed d spacing ± 0.001 (Å)			Integr. intensity +/−	Area per lipid mol. ± 0.1 ($Å^2$)	Primitive unit cell a, b, γ ± (0.002, 0.002, 0.2) (Å, Å, °)			Coherence length, L (Å)		Coherence length, L (Å) ± 1.0 Å	Tilt angle, t (°) ± 0.5	Tilt dir. from NN, non-symmetry (°) ± 2.0	σ (Å) ± 0.06	χ^2
Composition	$d_{1,0}$	$d_{0,1}$	$d_{1,-1}$			a	b	γ	$L_{1,0}$	$L_{0,1}$	$L_{1,-1}$				
DPPC	4.793	4.793	4.303	11,500	49.67	5.181	5.181	112.3	78 ± 10	78 ± 10	1,100[a] ± 100	19.0	34.3	0	0.6	9.3
DPPS	4.563	4.447	4.268	13,600	45.27	4.961	5.091	116.3	120 ± 10	140 ± 10	490 ± 20	16.1	29.5	6.0	0.9	10.7
DPPC:DPPS 90:10	4.737	4.737	4.297	7,400	48.79	5.150	5.150	113.1	75 ± 10	75 ± 10	1,300[a] ± 200	16.2	33.4	0	0.88	6.0
DPPC:DPPS 90:10 + PT (3 h)	4.742	4.742	4.298	7,540	48.87	5.153	5.153	113.0	75 ± 10	75 ± 10	500 ± 20	17.1	33.6	0	0.67	6.3
DPPC:DPPS 90:10 + PT (6 h)	4.766	4.766	4.766	7,590	49.27	5.168	5.168	112.7	80 ± 10	80 ± 10	425 ± 20	16.9	33.1	0	0.85	6.9

L_{xy} is the in-plane coherence length—an average size of the 2-D "crystalline" islands along the (x, y) crystallographic direction, L_c is the length of the coherently scattering part of the alkyl tail measured along its backbone

Symmetry direction: direction toward nearest neighbor

Integrated intensity is the combined intensity of {(0,1), (1,0)} and (1, −1) diffraction peaks

[a] Large uncertainty due to the instrumental resolution of the diffractometer

Table 1). Our experimental results showed that during the entire experiment there was a single gel phase without significant phase separation.

Presence of the purothionin causes a measurable increase in the 2-D unit cell dimensions of the ordered part of the DPPC:DPPS monolayer and in the average area per molecule (Table 1). The area per molecule in the ordered phase measured at ∼6 h after purothionin injection reaches almost the values for the pure DPPC monolayer. Additionally, the purothionin substantially decreases the order along the (1, −1) crystallographic direction from 1,300 to 425 Å, indicating that the packing of the phospholipid tails becomes more disordered. Although the packing of the ordered 2-D phase of the DPPC:DPPS phospholipid mixture becomes more disordered upon interactions with purothionin, the general shape of the in-plane diffraction patterns (GIXD) for the packing of the alkyl tails ($q_{xy} = 1.15$–1.55 $Å^{-1}$) does not change dramatically. Upon purothionin application (1) the protein does not form an ordered mono- or multilayer under DPPC:DPPS as exemplified by the absence of additional Bragg peaks at the lower q_{xy} region (0.08–1.15 $Å^{-1}$) where a signal from the protein might be expected (data not shown), (2) there is no indication that purothionin inserts into the DPPC:DPPS monolayer in a significant amount.

The X-ray reflectivity (XR) scattering data for 90:10 DPPC:DPPS monolayer and the same monolayer at ∼3 and ∼6 h after purothionin injection are shown in Fig. 7, and the comparison of the resulting electron density distributions are shown in Fig. 8 together with the electron density of pure DPPC. The modeling of the XR data provides complementary information about the behavior of the DPPC:DPPS monolayer interacting with purothionin. Here we present the results from the free form cubic b-spline fitting procedure (Hamley and Pedersen 1994) although the model dependent (stack of slabs) fitting resulted in similar electron density distributions (data not shown).

As in the case of GIXD, we measured the XR profiles for pure DPPC and DPPS monolayers (data not shown) and subsequently for a 90:10 mixture of DPPC and DPPS (Fig. 7). In all cases, the obtained electron density distributions (Fig. 8) clearly indicate the positions of the head groups and the alkyl chains vis-à-vis the liquid subphase.

The measurement performed 3 h after addition of purothionin shows dramatic changes in the XR (Fig. 7a vs. b) and the electron density profiles normal to the surface (Fig. 7b vs. b′) as compared to the pure DPPC:DPPS case. However, the measurement performed 6 h after purothionin injection resulted in the XR and electron density profiles that are closer to the mixed DPPC:DPPS monolayer without the protein present. Figure 8 shows the comparison between the electron density distribution for the mixed monolayer before and after the introduction of purothionin.

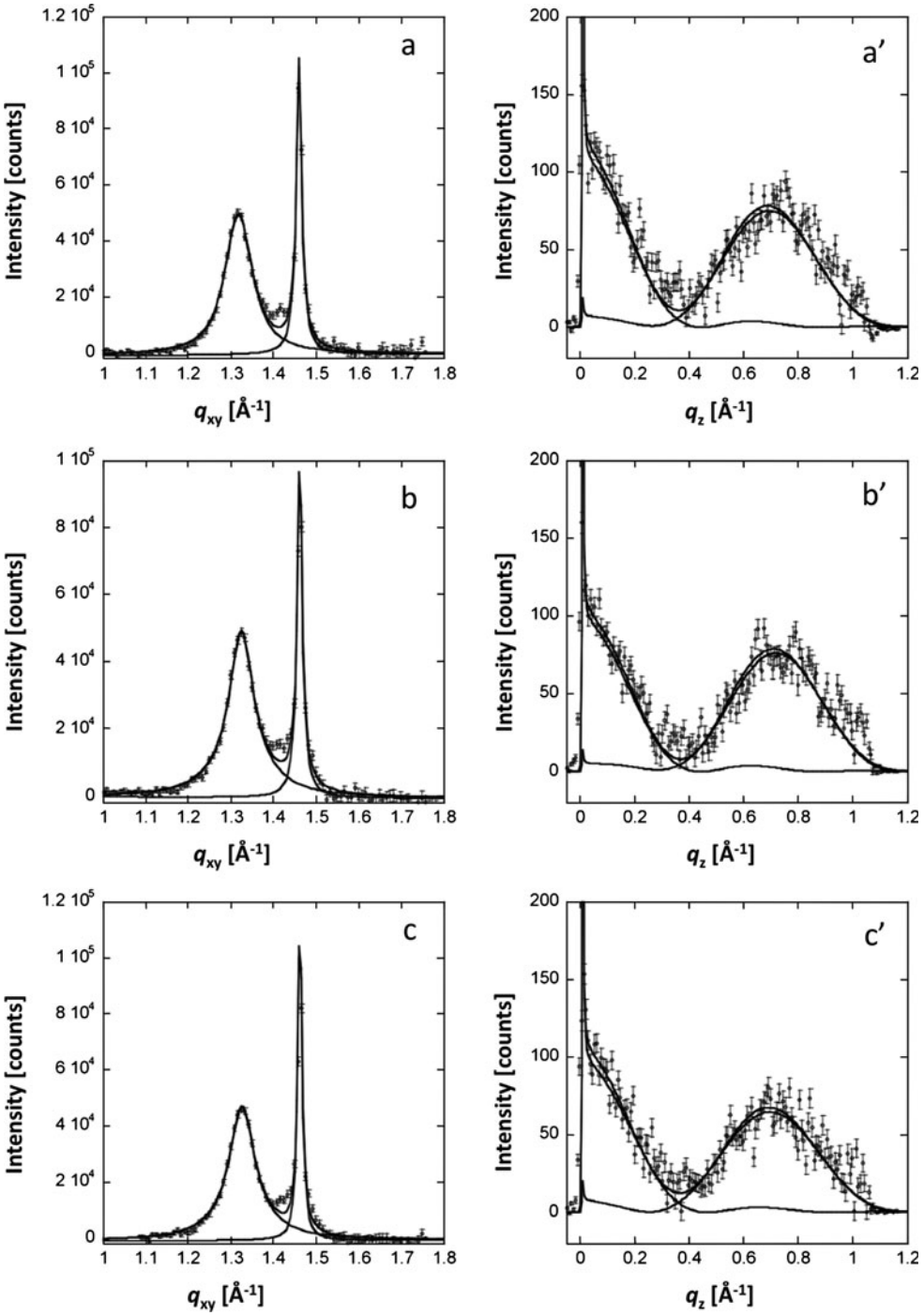

Fig. 6 GIXD profiles of pure 90:10 mol% DPPC:DPPS (**a**, **a**′) and the 90:10 mol% DPPC:DPPS ~3 h (**b**, **b**′) and ~6 h (**c**, **c**′) after injection of 5 mg/250 ml of purothionin. *Left panels* (**a**, **b**, **c**) represent Bragg peaks and the *right panels* (**a**′, **b**′, **c**′) show the Bragg rods. *Solid lines* represent the fits to the measured profiles, and the molecular packing parameters used in the fitting are listed in Table 1. Bragg peaks were obtained by integrating over the (-0.05 Å$^{-1} \leq q_z \leq 1.2$ Å^{-1}) region, and each peak was fit using a Voigt function (*solid lines*). By integrating over the (1.15 Å$^{-1} \leq q_{xy} \leq 1.55$ Å^{-1}) region, the Bragg rods were fitted (*solid line*) by approximating the coherently scattering part of the alkyl tail by a cylinder of length L_c and constant electron density

The electron density profile obtained after 3 h of purothionin incubation (green line in Fig. 8) shows a much broader head-group region and shorter tail region. There is much less distinction in electron density between the head-group region and the alkyl chains. This is most likely caused by a global disordering effect (increase in area per molecule in the liquid phase as well as lower percentage of lipids in ordered phase) caused by purothionin interactions. The disordering effect of the protein seems to be waning after ~4 h, and the membrane returns to a much more ordered state resembling, although not totally, a pure monolayer before the protein was injected. The shape of the electron density profile measured at ~6 h after protein injection resembles the profile of pure DPPC measured in the same conditions (blue vs. black line in Fig. 8). However, the integrated electron density is not preserved upon interaction with protein. This fact can be an indication that some rearrangement of the lipid monolayer took place and

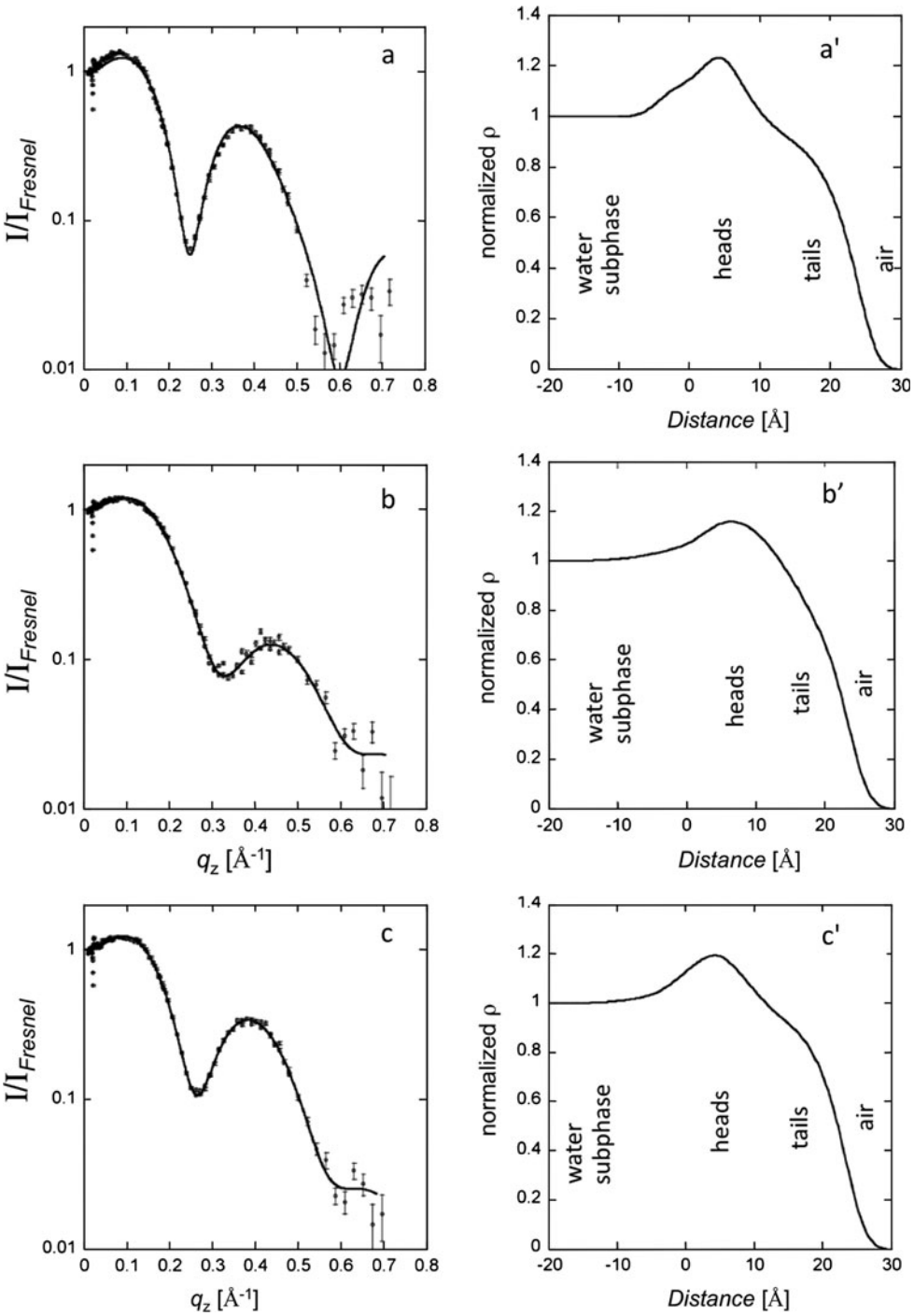

Fig. 7 X-ray reflectivity results for pure 90:10 DPPC:DPPS monolayer (**a**, **a**′), 90:10 DPPC:DPPS at ~3 h (**b**, **b**′) and at ~6 h (**c**, **c**′) after purothionin injection. All XR measurements were performed at 23°C on H_2O 50 mM Tris buffer subphase, pH = 8.2. **a**, **b**, **c** Measured reflectivity plotted as $R/R_{Fresnel}$ versus q_z. *Error bars* for the reflectivity data represent statistical errors in these measurements. Measured data are represented as *symbols*, and *solid lines* represent fits corresponding to the electron density profiles shown in **a**′, **b**′, **c**′. The electron densities *ρ(z)* are normalized to the electron density of water with buffer, ρ_{water} 0.338 $e^-/Å^{-3}$. In the electron density profiles, the DPPC:DPPS head-groups and alkyl tails can be clearly distinguished. Interaction with purothionin at ~3 h after injection results in a smearing of the electron density in the head-group and tail regions. At ~6 h after injection, the electron density profile changes towards the starting profile of the pure DPPC:DPPS monolayer

that some of the lipid molecules, most likely charged DPPS, were solubilized.

Discussion

How can we reconcile the fact that the GIXD spectra do not show the dramatic changes that XR spectra do? We should remember that the GIXD measures only the "ordered" part of the monolayer while XR coherently averages over both ordered and disordered components of the membrane (the coherence of the X-ray beam projected into the liquid surface extends to ~10 μm). Therefore, if the protein binds/interacts mostly with the disordered (or liquid) part of the system the biggest changes will be observed in the XR. Additionally, both GIXD as well as XR indicate that

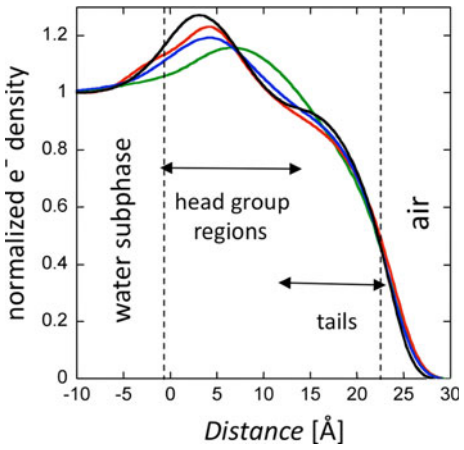

Fig. 8 Electron density profiles of the pure 90:10 DPPC:DPPS monolayer without purothionin (*red curve*) and at ~3 h (*green curve*) and ~6 h (*blue curve*) after purothionin injection. For comparison the electron density profile obtained for pure DPPC monolayer at 23°C and 20 mN/m (*black curve*) is also shown

after equilibrium is reached (~4 h after protein injection) the monolayer is reminiscent of a pure DPPC monolayer. Neither GIXD nor XR indicate any signature of substantial amounts of protein bound to the membrane. However, we should note that the membrane underwent reorganization during which a substantially larger proportion of the phospholipids shifted from the gel to the liquid phase. In order to account for the average 62 $Å^2$ per molecule established from the measurements of the area of the Langmuir trough and the amount of the spread lipid solution, the average area per molecule in the liquid phase must have a significantly larger value than 62 $Å^2$/molecule to account for an increase in the average from ~48 $Å^2$/molecule as established in the gel phase by GIXD method.

In recent years three competing hypotheses have emerged for mechanisms of thionin interaction with the membrane. The first hypothesis proposed a formation of ion channels spanning the membrane and being controlled by the membrane potential. Those channels are supposed to lead to ionic imbalance and membrane rupture. This hypothesis would require a significant change in monolayer properties as probed by our experiments. It would require a major increase in surface pressure as well as the presence of a significant amount of protein in the monolayer. Additionally it is likely that emerging protein channel architecture would be associated with the ordered part of the membrane therefore significantly changing the GIXD spectra. None of those changes were observed in our model system discussed in this paper. Unequivocal observation of the ion channel formation will require new sets of experiments in the presence of the full lipid bilayer structure in a liquid environment. A monolayer at the air-liquid interface is not an ideal model system to follow such processes although the preliminary stages of the protein insertion into the single layer should be detectable. Additionally, Thevissen et al. (1999) questioned the channel formation hypothesis on the grounds that the compounds with significant sizes such as antibiotics and fluorescent dyes passed through the membrane unhindered.

The second proposal suggested a formation of protein patches or rafts on top of the membrane. Such a structure would again lead to a substantial increase in electron density associated with the presence of the protein under the model membrane. Since the shape of purothionin can be approximated as a hemisphere with a radius of 15–20 Å such length scales should be readily detectable via XR assuming that the surface occupancy of the protein exceeds 5% of the monolayer surface. Additionally such an arrangement could possibly lead to a separate GIXD signal for ordered proteins as they are adsorbed at the surface of the membrane (Miller et al. 2008a, b). Again no such changes were observed in the present work.

The third proposal suggested that the protein is loosely and transiently associated with the membrane and that very high protein solubility (~330 mg/ml) leads to a withdrawal of a significant portion of anionic phospholipids (in our case DPPS) and their effective solubilization. Such a mechanism should promote membrane disorganization, lower the percentage of membrane in the gel phase, and lead to a pure component membrane composition. Most of those expectations were realized in the course of our experiment. Hence the results presented in the paper provide a tentative support for this hypothetical mechanism.

Additionally, the results provide even more strict limitations on possible lytic mechanisms. Richard et al. (2002) suggested that the protein should interact with the membrane in such a fashion that the helices should form a ~60° angle with the membrane surface and beta sheets ~30°. A quick inspection shows that the model proposed by him has two rather than a single solution as presented in the original paper. The reversal of the molecule direction coincides with the direction suggested by Fig. 1. The direction of the electromagnetic field (red arrow) coincides with the normal to the membrane and leads to the fulfillment of both angular conditions. Such a direction would also bring Tyr13 into proximity to the membrane, iodination of which abolishes the lytic activity (Fracki et al. 1992). As suggested before (Richard et al. 2002, 2005), the introduction of the protein increases the disorder of the membrane and leads to opposing effects: rigidifying of the already existing gel phase and liquefying of the rest of the membrane. Both effects result in changes in the integrity of the membrane leading to leakage and eventual destruction of the membrane. Therefore the data supporting the third mechanism explain how the two other competing hypotheses are transiently realized.

Conclusions

We studied the interaction of purothion with the two component, DPPC:DPPS, monolayers at the liquid-air interface using synchrotron X-ray scattering. The GIXD showed an increase in area per molecule in the ordered (gel) phase of the monolayer and a decrease in the amount of the monolayer's ordered phase caused by the protein. The XR showed significant but transient changes in the electron density distribution of the monolayer perpendicular to the interface upon application of the protein, but the modeled electron density did not show any significant contribution from bound protein. Assuming that the monolayer conditions reflect well the environment in which the purothionin toxins act, the results significantly limited the possible models for the lytic activity of the thionins. The results appear to be most consistent with the model in which proteins transiently bind to the surface of phospholipids in the liquid phase and solubilize some of them. The results presented in this paper seem to be incompatible with ion channel formation models or the protein raft model although additional studies, perhaps with bilayers at the solid–liquid interface (Miller et al. 2008c), are required to prove this hypothesis.

The effect of purothionin on the monolayer structure is complex. A substantial removal of the DPPS component of the monolayer by purothionin will require a decrease in the average area per molecule. In the case when all DPPS molecules would be removed, the area per molecule should decrease by $\sim$10% in agreement with the mol% of this component in the monolayer. Additionally, the integrated intensity of the Bragg diffraction peaks should increase, reaching the intensity of the pure DPPC component. However, a different trend was observed. The average area per molecule, as measured by the expanding barrier in the Langmuir trough, increased by $\sim$7% (Fig. 4). The GIXD suggests (Table 1) that as time progresses, the ordered portion of the DPPC:DPPS monolayer that originally had unit cell parameters significantly different from the pure DPPC phase is getting closer to the parameters of the ordered part of the pure DPPC monolayer. However, such a 1% increase cannot explain the increase in the total area per molecule as measured by the GIXD in the ordered phase of the monolayer. The translocation of a significant number of phospholipid molecules from the gel to liquid phase offers such an explanation. The decrease in size of the gel phase rafts combined with restoration of the physical characteristics of the pure DPPC gel phase and electron density obtained in the XR studies provides additional support for such an interpretation.

The final values of the length of the coherently scattering monolayer domains in the (1, -1) crystallographic direction are almost half of those of the pure DPPC and DPPC:DPPS monolayers. The decrease in the integrated intensities of the Bragg peaks as compared with pure DPPC suggests that the ordered phase of the resulting monolayer has approximately half of the ordered domains of the pure DPPC at the same surface pressure. The purothionin did cause the loss of DPPS from the ordered phase but also created a shift in the remaining DPPC composition from the gel to the disordered phase. Although the remaining gel phase increased the average unit cell size by about 1%, the total increase in area per molecule can be explained by the increase in the amount of the liquid phase of DPPC. Such an increase in the internal disorder should be followed by an increase in water penetration into the head-group region of the monolayer. The effect of the monolayer disordering is even more pronounced in the XR measurements. The decrease in total thickness of the monolayer (measured between the inflection points of the electron density distribution at the air/tail and head-group/subphase interfaces) along the surface normal testifies to a much greater average molecular tilt of molecules in the assembly during the transition.

Experiments with fluorescently labeled phosphoserine (Stec et al. 2004) suggested that $\sim$10% purothionin remains associated with the membrane while almost 90% is shifted to the aqueous phase with lipids bound. This fact may provide an alternative explanation for the increase in the averaged area per molecule. Both described effects explain an apparent discrepancy between a loss of DPPS from the membrane and the sizable ($\sim$7%) increase in the total surface of the membrane. However, this behavior is fully within the range of expected membrane behavior leading to the appearance of blebs and holes visible in electron micrographs (Oka et al. 1992). Therefore, the results described in this work clearly support the solubilization mechanism of membrane permeabilization.

Acknowledgments The work was supported by the Los Alamos National Laboratory under the auspices of the United States Department of Energy under DOE contract W7405-ENG-36, and by the DOE Office of Basic Energy Science. We thank Dr. Kristian Kjaer from the University of Copenhagen in Denmark who collaborated with us on the GIXD and XR measurements at HASYLAB, Hamburg, Germany.

References

Als-Nielsen J, Jacquemain D, Kjaer K, Leveiller F, Lahav M, Leiserowitz L (1994) Principles and applications of grazing incidence X-ray and neutron scattering from ordered molecular monolayers at the air-water interface. Phys Rep 246:251–313

Angerhofer CK, Shier WT, Vernon LP (1990) Phospholipase activation in the cytotoxic mechanism of thionin purified from nuts of pubera. Toxicon 28:547–557

Bohlmann H, Apel K (1991) Thionins. Annu Rev Plant Physiol 42:227–240

Broekaert WF, Cammue BPA, Debolle MFC, Thevissen K, Desamblanx GW, Osborn RW (1997) Antimicrobial peptides from plants. Crit Rev Plant Sci 16:297–323

Carrasco L, Vazquez D, Hernandez-Lucas C, Carbonero P, Garcia-Olmedo F (1981) Thionins: plant peptides that modify membrane permeability in cultured mammalian cells. Eur J Biochem 116:185–189

Castro MS, Fontes W (2005) Plant defense and antimicrobial peptides. Prot Pept Lett 12:13–18

Debreczeni JE, Girmann B, Zeeck A, Kratzner R, Sheldrick GM (2003) Structure of viscotoxin A3: disulfide location from weak SAD data. Acta Cryst D 59:2125–2132

Evans JE, Wang Y, Shaw KP, Vernon LP (1989) Cellular responses to Pyrularia thionin are mediated by Ca^{2+} influx and phospholipase A2 activation and are inhibited by thionin tyrosine iodination. Proc Nat Acad Sci USA 86:5849–5853

Fracki WS, Li D, Owen N, Perry C, Naisbitt GH, Vernon LP (1992) Role of Tyr and Trp in membrane responses of Pyrularia thionin determined by optical and NMR spectra following Tyr iodination and Trp modification. Toxicon 30:1427–1440

Garcia-Olmedo F, Molina A, Alamillo JM, Rodriguez-Palenzuela P (1998) Plant defense peptides. Biopolymers 47:479–491

Giudici M, Pascual R, de la Canal L, Pfuller K, Pfuller U, Villalain J (2003) Interaction of viscotoxins A3 and B with membrane model systems: implications to their mechanism of action. Biophys J 85:971–981

Guinier A (1963) X-ray diffraction. Freeman, San Francisco

Hamley IW, Pedersen SJ (1994) Analysis of neutron and X-ray reflectivity data. I. Theory. J Appl Crystallogr 27:29–35

Huang W, Vernon LP, Bell JD (1994) Enhancement of adenylate cyclase activity in S49 lymphoma cell membranes by the toxin thionin from Pyrularia pubera. Toxicon 32:789–797

Hughes P, Dennis E, Whitecross M, Llewellyn D, Gage P (2000) The cytotoxic plant protein, beta-purothionin, forms ion channels in lipid membranes. J Biol Chem 275:823–827

Jensen TR, Balashev K, Bjørnholm T, Kjaer K (2001) Novel methods for studying lipids and lipases K and their mutual interaction at interfaces. Part II. Surface sensitive synchrotron X-ray scattering. Biochimie 83:399–408

Johnson KA, Kim E, Teeter MM, Suh SW, Stec B (2005) Crystal structure of alpha-hordothionin at 1.9 Angstrom resolution. FEBS Lett 579:2301–2306

Li SS, Gullbo J, Lindholm P, Larsson R, Thunberg E, Samuelsson G, Bohlin L, Claeson P (2002) Ligatoxin B, a new cytotoxic protein with a novel helix-turn-helix DNA-binding domain from the mistletoe Phoradendron liga. Biochem J 366:405–413

Llanos P, Henriquez M, Minic J, Elmorjani K, Marion D, Riquelme G, Molgo J, Benoit E (2004) Neuronal and muscular alterations caused by two wheat endosperm proteins, puroindoline-a and alpha1-purothionin, are due to ion pore formation. Eur Biophys J 33:283–287

Mansour HM, Zografi G (2007) Relationships between equilibrium spreading pressure and phase equilibria of phospholipid bilayers and monolayers at the air-water interface. Langmuir 23:3809–3819

Miller CE, Busath DD, Strongin B, Majewski J (2008a) Packing of ganglioside GT1b:DPPE and DPPC phospholipid mixtures at the air-liquid interface. An X-ray reflectivity and grazing incidence diffraction study. Biophys J 95:641–647

Miller CE, Majewski J, Watkins EB, Kuhl TL (2008b) Part I: an X-ray scattering study of cholera toxin penetration and induced phase transformations in lipid membranes. Biophys J 95:629–640

Miller CE, Majewski J, Watkins EB, Mulder DJ, Gog T, Kuhl TL (2008c) Probing the local order of single phospholipid membranes using grazing incidence X-ray diffraction. Phys Rev Lett 100:058103

Neville F, Ishitsuka Y, Hodges CS, Konovalov O, Waring AJ, Lehrer R, Lee KY, Gidalevitz D (2008) Protegrin interaction with lipid monolayers: grazing incidence X-ray diffraction and X-ray reflectivity study. Soft Matter 4:1665–1674

Oka T, Murata Y, Nakanishi T, Yoshizumi H, Hayashida H, Ohtsuki Y, Toyoshima K, Hakura A (1992) Similarity, in molecular structure and function, between the plant toxin purothionin and the mammalian pore-forming proteins. Mol Biol Evol 9:707–715

Rao U, Stec B, Teeter MM (1995) Refinement of purothionins reveals the solute particles important for the lattice formation and toxicity. Part 1: α1-purothionin revisited. Acta Cryst D51:904–913

Richard JA, Kelly I, Marion D, Pezolet M, Auger M (2002) Interaction between beta-purothionin and dimyristoylphosphatidylglycerol: a (31)P-NMR and infrared spectroscopic study. Biophys J 83:2074–2083

Richard JA, Kelly I, Marion D, Auger M, Pezolet M (2005) Structure of beta-purothionin in membranes: a two-dimensional infrared correlation spectroscopy study. Biochemistry 44:52–61

Stec B (2006) Plant thionins-the structural perspective. Cell Mol Life Sci 63:1370–1385

Stec B, Rao U, Teeter MM (1995) Refinement of purothionins reveals the solute particles important for the lattice formation and toxicity. Part 2: structure of β-purothionin at 1.7 Å resolution. Acta Cryst D51:914–924

Stec B, Markman O, Rao U, Heffron G, Henderson S, Vernon LP, Brumfeld V, Teeter MM (2004) Proposal for molecular mechanism of thionins deduced from physico-chemical studies of plant toxins. J Pept Res 64:210–224

Thevissen K, Terras FRG, Broekaert WF (1999) Permabilization of fungal membrane by plant defensins and thionins inhibits fungal growth. Appl Environ Microbiol 65:5451–5458

Vernon LP, Bell JD (1992) Membrane structure, toxins and phospholipase A2 activity. Pharmacol Ther 54:269–295

Woynarowski JM, Konopa J (1980) Interaction between DNA and viscotoxins cytotoxic basic polypeptides from Viscum album. L Hoppe Seylers Z Physiol Chem 361:1535–1545